Observation and analysis of core-penetrating Rydberg states of calcium monofluoride

John M. Berg,* James E. Murphy,† Nicole A. Harris, and Robert W. Field‡
Department of Chemistry, Massachusetts Institute of Technology, Cambridge, Massachusetts 02139
(Received 24 November 1992; revised manuscript received 19 April 1993)

Optical-optical double-resonance fluorescence excitation spectra of molecular Rydberg states of CaF are reported, and states up to 45 500 cm^{-1} above the $X\,^2\Sigma^+$ ground state are rotationally analyzed. The new electronic states are arranged into six "core-penetrating" Rydberg series by fitting their energies to the Rydberg equation using effective principal quantum numbers. The ionization potential of CaF is thereby determined to be 46 998±5 cm^{-1}. Spin-orbit, Λ-doubling, and spin-rotation constants are determined for a subset of the observed states. Scaling relationships for each of these fine-structure effects are developed and shown to yield characteristic scaling parameters for each series. Analysis, using Ca^+ atomic orbitals as a basis set for the molecular Rydberg orbitals, shows that each of the six observed molecular Rydberg series correlates with a core-penetrating Rydberg series of the Ca^+ ion, and that the $p \sim d$ mixing suggested by the spin-orbit scaling parameters of the $^2\Pi$ states is consistent with that previously determined for low-lying states using a ligand-field model. The spin-orbit scaling parameter for the lone $^2\Delta$ series is consistent with pure $l=2$ character. In the lowest-lying state of each series, $n \sim (n+1)$ mixing is shown to account for deviations of the molecular constants from scaling predictions based on the corresponding constants of the higher-lying states. The coefficients of scaling relations for the Λ-doubling and spin-rotation constants reveal interseries interactions which are consistent with substantial l mixing and which suggest that multistate perturbation and/or multichannel quantum-defect analyses should be pursued.

PACS number(s): 33.10.Lb, 35.20.Sd, 35.20.Vf, 33.40.Ta

I. INTRODUCTION

Calcium monofluoride is unique among molecules whose Rydberg states have been studied spectroscopically. It has both a closed-shell ($^1\Sigma^+$) ion core consisting of two closed-shell atomic ions, Ca^{2+} and F^-, and a large core dipole moment. In a recent letter we reported the observation of transitions to low and intermediate Rydberg states of the CaF molecule by optical-optical double-resonance (OODR) fluorescence excitation spectroscopy [1]. The purpose of this paper is to describe those results in detail and to focus on the fine structure within each state to gain insights into the electronic structure.

Emphasis will be placed on determining scaling relationships as compact descriptions of the properties of the large number of observed states. The scaling coefficients will be shown to be characteristic properties of each group of states collectively identified as a Rydberg series. This reduction of a large body of data to a few parameters will serve as the entry into an examination of the underlying physics which produces the observed electronic structure and the relationship of the present observations on Rydberg states to the models which have been applied to the low-lying valence states.

The bonding interaction in CaF and the other alkaline-earth monohalide diatomic molecules has been treated as an electrostatic attraction between the M^{2+} and X^- atomic ions. The single electron outside of the closed-shell cores of these two atomic ions has been assumed to occupy a metal-centered orbital which is perturbed by the presence of the halide ion. The properties of the valence electron in the X, A, B, and C states have been treated by Rice, Martin, and Field [2] (RMF) using a ligand-field model and by Törring, Ernst, and Kändler [3] (TEK) using an electrostatic polarization model. Recent experimental work by others has completed the identification of the next group of states to higher energy, including the observation of the lowest-lying $^2\Delta$ state by d'Incan *et al.* [4], the reassignment of the reported $D\,^2\Sigma^+$ state to $v=1$ of $C'\,^2\Sigma^+$ [5], and the observation of the next-higher-energy $v=0$ $^2\Sigma^+$ state (above the $E^2\Sigma^+$) which turns out to be the lowest-energy member of one of the three $^2\Sigma^+$ series described here [6]. The most current spectroscopic information on all states of the CaF molecule not observed originally by us is summarized in Table I. Our analysis will show that this list includes *all* of the core-penetrating states which are expected in the $T_0 \leq 37\,600$ cm^{-1} energy range.

The focus of this paper is on the analysis of the Rydberg states lying at higher energy, $40\,000 < T_0 < 45\,500$ cm^{-1}, than the states listed in Table I. Our approach to the analysis consists of several stages. In the first stage we determine the value of Λ for each state by examining the rotational line patterns at low J'. The absence of certain diagnostically important lines provides the key Λ-assignment information. In the second stage we determine v by comparing OODR excitation spectra out of $v'=0$ and 1 levels of the $A\,^2\Pi$ intermediate state, carefully measuring $\Delta G_{1/2}$ for selected Rydberg states, and identifying such intervals in the spectra. Then, in the third stage we arrange states of the same v and Λ into series, the energies of which converge to a common ionization limit (E_{IP}) according to the modified Rydberg

TABLE I. Molecular constants for the low-lying states of CaF.

	T_0	$\Delta G_{1/2}$	B_0	γ	A_{SO}	p	q	n^*	Nominal Ca^+ nl	Reference
$X\,^2\Sigma^+$	0.000	589	0.3425	+0.0013				1.528	4s	[22]
$A\,^2\Pi$	16 529.689	595	0.348		71.450	−0.044 54	-2.97×10^{-4}	1.898	4p	[10,14]
$B\,^2\Sigma^+$	18 841.309	572	0.3425	−0.045 81				1.974	3d	[23]
$B'\,^2\Delta$	21 543.893	523	0.328		12.398			2.076	3d	[4,24]
$C'\,^2\Sigma^+$	30 158.617	656	0.3654	+0.0021				2.553	5s	[5]
$C\,^2\Pi$	30 215.949	482	0.3233		29.320	0.001 1	-1.08×10^{-4}	2.557	3d	[5]
$E\,^2\Sigma^+$	34 171.218	648	0.3632	+0.0557				2.925	4d	[26]
$E'\,^2\Pi$	34 477.413	675	0.367		16.483	0.053 04	7.74×10^{-4}	2.959	5p	[26]
$[^2\Delta]$[a]	35 650±150				3			~3.11	4d	
$F'\,^2\Sigma^+$	36 125.976	693	0.3732	−0.0066				3.177	4p	[6]
$F\,^2\Pi$	37 604.597	676	0.360		9.184	0.000 35	2.20×10^{-4}	3.418	4d	[6,27]

[a]This state is predicted by the present work, but has not been observed.

equation

$$E_{n^*}=E_{IP}-\frac{R_{CaF}}{n^{*2}} \tag{1}$$

where n^* is the effective principal quantum number, differing from the principal quantum number by the quantum defect μ according to $n^*=n-\mu$, and R_{CaF} is the Rydberg constant corrected for the noninfinite mass of CaF^+ ($R_{CaF}=109\,736.3\ cm^{-1}$). Since the ionization potential of the molecule is unknown initially, this is an iterative process in which E_{IP} is adjusted until the value is found which best allows all of the observed states to be assigned to series having nearly constant values of μ. In the fourth and final stage of the initial analysis, the series assignments are confirmed by showing that the molecular constants which we have measured for each state vary sensibly along each series. Comparisons of measured spin-orbit, Λ-doubling, and spin-rotation constants are most useful in this regard.

Up to this point the analysis requires no assumptions about the behavior of the Rydberg states other than that the energies should scale according to Eq. (1) with approximately constant quantum defects within a series. This assumption must be valid for sufficiently large n^* since the molecular-ion core will inevitably appear more like a +1 point charge as n^* increases. After identifying the Rydberg-series structure using this empirical approach, we proceed to develop a unified physical understanding of the core-penetrating series of electronic states. Each of these series can be followed to its terminus among the "valence" states modeled by RMF and TEK. Core-penetrating CaF Rydberg series are derived from core-penetrating Ca^+ atomic ion states with $l\leq2$. Atomic states with $l\geq3$ are kept out of the core by the centrifugal barrier in the effective atomic potential. (Note that the l values that are expected to be associated with core-penetrating series depend on the row of the Periodic Table: Be^+,Mg^+ $l\leq1$; Ca^+,Sr^+ $l\leq2$; Ba^+ $l\leq3$.) An operational definition of a core-penetrating Rydberg series is $\mu\geq0.05$ (although a Rydberg series with integer μ can accidentally become nonpenetrating). The physical significance of core-penetrating Rydberg series is that most of the important coupling between different Rydberg series (l mixing) or exchange of energy between the Rydberg electron and the core electrons or nuclear motions (rotation and vibration) occurs when the Rydberg electron penetrates inside the ion core (as distinct from long-range Rydberg-core interactions).

It is a well-known consequence of the normalization condition that the amplitude of the innermost lobe of a Rydberg orbital is proportional to $n^{*-3/2}$ [7]. Thus, if the most important Rydberg-core interactions are controlled by core penetration, it is reasonable to expect that many properties of core-penetrating molecular Rydberg series will be described by n^*-based scaling relationships. The primary hypothesis being explored here is that scaling relations can be developed which describe properties other than electronic energies in the same compact manner that Eq. (1) describes the energies. The characteristics of an entire series may then be determined by detailed analysis of only a few states which belong to the series. Only the scaling parameter n^* and the empirically determined, series-specific scaling coefficients are needed in order to predict the properties of any Rydberg state. Our discussion will be divided between a demonstration that scaling relations hold for spin-orbit, Λ-doubling, and spin-rotation constants, followed by the use of the characteristic scaling coefficients determined for each series to connect our understanding of the Rydberg series with the models developed for the valence states.

Scaling relationships for the spin-orbit interaction will be developed by analogy with spin-orbit interactions in atomic Rydberg states. The scaling factors will show quantitatively that the l mixing of Ca^+ atomic orbitals calculated by RMF for low-lying states persists in the innermost lobes of all Rydberg orbitals which belong to the same series. The retention of the form of the innermost lobes throughout each series is discussed by Mulliken [8]. Scaling relations for l-uncoupling interactions will be developed by adjusting the scaling coefficients from those expected under the hypothesis of pure l states. The observed Λ-doubling and spin-rotation parameters will provide insights into which series interact with each other most strongly. These fine-structure parameters will serve as indicators of supercomplex formation, a phenomenon which we are currently exploring and will discuss in a future publication [9].

II. EXPERIMENT

The rovibronic energy levels of a diatomic molecule become extremely congested in the intermediate and high Rydberg regions, particularly due to rotational structure when one or both of the constituent atoms are relatively heavy. Direct, one-photon excitation of these states from thermally populated levels of the ground or low-lying states normally produces spectra which are difficult or impossible to interpret because the spectral density of observed transitions is too high for reliable assignments to be made. One of the ways to reduce the spectral complexity of these systems is to cool the molecules, limiting the initial states to the lowest rovibronic levels. Another method is to use optical-optical double resonance to restrict the number of rotational levels which are accessible in a given experiment. Bernath and Field used this latter technique to study the E and E' states of CaF, employing two continuous-wave dye lasers and using the $A\,^2\Pi$ state as the intermediate state [10]. We use OODR in this work, but we employ pulsed dye lasers to produce the wavelengths necessary to reach the Rydberg states.

The OODR technique has the advantage of allowing access to selected, diagnostically important high rotational levels which would not be populated in a cooled system. The high rotational levels are interesting for what they reveal about interactions between Rydberg levels as a function of rotation-vibration quantum numbers of the molecular ion core. They allow determination of Λ-doubling parameters and spin-rotation parameters, which are manifestations of interactions between remote states in the most common effective-Hamiltonian models used to describe diatomic molecular spectra.

Molecular CaF is produced by heating a mixture of CaF_2 (crystalline) and either Ca metal (turnings) or boron (powder) in a graphite crucible to 1400 °C under 200 mTorr of flowing argon. The region about 1 cm above the mouth of the crucible is probed with the overlapping region of two nearly collinear pulsed-dye-laser beams. One beam, the pump, is tuned to a single rovibronic transition in the $A\,^2\Pi - X\,^2\Sigma^+$ band. This excites a single J and parity-selected level of the $A\,^2\Pi$ state, with the flexibility to choose nearly any rotational level which is thermally populated in the ground state. A second beam, the probe, excites molecules from the rovibronic level of $A\,^2\Pi$ selectively populated by the pump to rovibronic levels of Rydberg states as its frequency is tuned. Since the $A\,^2\Pi \leftarrow X\,^2\Sigma^+$ pump transition results in the population of a single-parity component of one $A\,^2\Pi$ rotational level, subsequent probe transitions to Rydberg states are both J selected and parity selected. For most of our experiments, the pump beam is produced by using a Nd:YAG laser (where YAG denotes yttrium aluminum garnet) to pulse amplify the output of a Coherent 699-21 ring dye laser (linewidth <0.005 cm^{-1}). Near the end of this series of experiments we changed our pump laser from a pulse-amplified Coherent 699-21 dye laser to a Nd:YAG-pumped Spectra Physics pulsed dye laser (PDL-1). This system is easier to operate and provides a wider range of pump wavelengths. The probe beam is the frequency-doubled output of a Lambda Physik FL3002E pulsed dye laser (linewidth ≈ 0.03 cm^{-1}) pumped by the same Nd:YAG laser.

Rydberg state $\leftarrow A\,^2\Pi$ transitions are detected by collecting and measuring the ultraviolet (uv) fluorescence ($\sim$240–220 nm) produced by radiative decay from the Rydberg manifold to $X\,^2\Sigma^+$. The decay process is probably some combination of direct radiative decay from the initially excited state and a cascade process involving radiative and collision-induced decay to lower states in the Rydberg manifold followed by radiative decay to $X\,^2\Sigma^+$. Only photons from those radiative transitions which terminate in the ground state are detected in our apparatus. These are not likely to be efficient processes, but because there are no other significant sources of such short-wavelength fluorescence in our experiment, this detection method produces the best signal-to-noise ratios for the energy regions we have probed thus far. We have also obtained spectra by detecting depletion of $A\,^2\Pi \rightarrow X\,^2\Sigma^+$ fluorescence when the probe laser is in resonance with a Rydberg $\leftarrow A\,^2\Pi$ transition. This is similar to the fluorescence dip technique employed in stimulated emission pumping experiments [11], but without the dual-beam null scheme. Over the energy range where fluorescence-depletion detection was used, all of the same transitions are observed as in uv-fluorescence detection, but the relative intensities are different and the signal-to-noise ratio is inferior. Furthermore, we have encountered interfering fluorescence in some spectral regions due to an uncharacterized excitation process involving only the probe beam when using the fluorescence depletion method.

The uv fluorescence is detected in a direction perpendicular to the laser propagation direction by a solar-blind photomultiplier tube (PMT) behind a bandpass interference filter. The signal current is converted to a voltage and processed with a gated integrator (typical gate width of 150 ns and gate delay of 15 ns) to minimize noise from the residual laser scatter which reaches the PMT. Resulting signals are digitized and stored in a microcomputer as the probe laser wavelength is scanned. Fluorescence lifetimes range from 100 ns to more than 1 μs, depending upon the Rydberg state being excited. Since we do not observe significant variations in fluorescence decay rates following excitation of different rotational levels of the same electronic state, no attempt has been made to correct line intensities by normalizing for differences in lifetime or fluorescence quantum yield. Our fluorescence signal disappears for Rydberg states with n^* values just above $n^* = 10$ (46 000 cm^{-1}). This is above the dissociation limit (44 200 cm^{-1}) [12]. Predissociation is a possible explanation for the disappearance of uv fluorescence above $n^* = 10$. Alternatively, our detection scheme may no longer be efficient at $n^* > 10$ because the spontaneous fluorescence rates become too slow to compete with unimolecular dissociation or collision-induced dissociation or ionization.

The common data set for all the Rydberg states that we have studied is that of probe transitions out of $J' = 3.5f$ and $1.5f$ of $A\,^2\Pi_{3/2}$ $v = 0$ excited via $A\,^2\Pi_{3/2} - X\,^2\Sigma^+$ $Q_2(3.5)$ and $Q_2(1.5)$ pump transitions. The $J = 2.5f$ Rydberg rotational level can be accessed by

both of these excitation paths, thus providing an automatic energy linkage of the two sets of spectra. These low-J data allow us to determine the value of the Λ quantum number and the spin-orbit coupling parameter (A_{SO}). Assuming Hund's case (b) Rydberg states and unresolved spin-rotation splitting and Λ doubling, transitions out of the $A\,^2\Pi_{3/2}, J'=3.5f$ ($N'=4$) intermediate level give a two-line pattern separated by $2B(2N'-1)$ for $^2\Sigma^+$ Rydberg states and give a four-line pattern with intervals of $2B(N'-1)$, $2BN'$, and $2B(N'+1)$ for both $^2\Pi$ and $^2\Delta$ Rydberg states. (Note that B is the rotational constant of the Rydberg state and N' is the total angular momentum exclusive of spin of the pumped $A\,^2\Pi$ level.) Transitions out of $A\,^2\Pi_{3/2}, J'=1.5f$ ($N'=2$) give the same two-line and four-line patterns for the $^2\Sigma^+$ and $^2\Pi$ states, but for $^2\Delta$ states only three lines are observed. The lowest-energy rotational line is missing for $^2\Delta$ states because they have no $J=0.5$ ($N=1$) level. In addition, the relative rotational line intensities are useful diagnostics for distinguishing between $^2\Pi$ and $^2\Delta$ states. The extreme lines of the four-line pattern are weaker relative to the middle two lines for transitions to $^2\Delta$ states than they are for transitions to $^2\Pi$ states. This occurs because the Q branches are strongly allowed for the $\Delta\Lambda\neq 0$ transitions. The intensity patterns are also sensitive to the value of A_{SO} [13], which is a useful diagnostic when the spin-orbit splittings of rotational lines in near-case (b) states are poorly resolved.

Further experiments, involving pumping higher J' (up to 46.5) or other branches of the $A\,^2\Pi - X\,^2\Sigma^+$ transition in order to access Rydberg-state rotational levels of the opposite parity, have been performed for many of the Rydberg states discussed here. These larger data sets have been used to derive B values, Λ doubling, and spin-rotation constants. A nonlinear least-squares fitting program has been used to fit the Rydberg state $\leftarrow A\,^2\Pi$ transition frequencies. Only the molecular constants that define the effective Hamiltonian for the Rydberg states were varied. The $A\,^2\Pi$ state molecular constants were held fixed at the values determined by Bernath and Field [10] in fitting their OODR data and the A-X data of Nakagawa *et al.* [14].

III. RESULTS

The set of spectroscopic data obtained by uv-fluorescence-detected OODR includes transitions to over 60 new vibronic states. The measured molecular constants for most of these states are summarized in Tables II–IV and described below. We find that the numbers of observed $^2\Sigma^+$, $^2\Pi$, and $^2\Delta$ vibronic states are in the approximate proportions of 3 to 2 to 1. This is what would be expected if transitions into *all* Rydberg states correlating with $l\leq 2$ (s, p, and d) states of a spherical ion core yet *no* higher-l states were excited. Interaction with the axial field of the molecular core splits a d Rydberg orbital into $^2\Sigma^+$, $^2\Pi$, and $^2\Delta$ states, splits a p orbital into $^2\Sigma^+$ and $^2\Pi$, and gives $^2\Sigma^+$ from an s orbital. We thus expect to observe six series of states originating from core-penetrating Ca^+ orbitals. The relative Λ abundances are consistent with our having observed only these core-penetrating series.

The ionization potential in Eq. (1) is the difference between the energy of the $X\,^2\Sigma^+$ $v=0$, $N=0$ rovibronic state of CaF and that of a free, zero-kinetic-energy electron plus the CaF^+ ion core in $X\,^1\Sigma^+ v=0$, $J=0$. Implicit in the use of Eq. (1) for determining E_{IP} is the assumption that all of the Rydberg state energies used are those of $v=0$ vibrational levels. However, the large difference in vibrational frequency between the $A\,^2\Pi$ state ($\omega_e=595$ cm^{-1}) and intermediate-n^* Rydberg states ($\omega_e\approx 680$ cm^{-1}) suggests that the OODR spectra recorded out of $A\,^2\Pi$ $v'=0$ should contain a significant number of lines due to $\Delta v\neq 0$ Rydberg state $\leftarrow A\,^2\Pi$ transitions. A simple Franck-Condon calculation using the assumed characteristic Rydberg-state vibrational frequency confirms this expectation. The $v=0$ levels must be identified definitively before proceeding with the analysis.

The $v=0$ Rydberg levels in our OODR spectra recorded out of $A\,^2\Pi$ $v'=0$ are identified primarily by searching for series of transitions with the spacing of the estimated Rydberg vibrational frequency and assigning them to vibrational progressions of single Rydberg states. The lowest-energy observed member of each series is taken to be the transition terminating on $v=0$. The vibrational assignments are supported by collecting a second, more limited set of spectra out of $A\,^2\Pi v'=1$ and comparing these spectra with the original spectra. The $v'=1$ spectra are nearly identical to those recorded out of $A\,^2\Pi$ $v'=0$, but are shifted in energy by the difference between the vibrational frequencies of the Rydberg state and the $A\,^2\Pi$ state. The major difference between the spectra out of $v'=1$ compared with those out of $v'=0$ is that $\Delta v=-1$ transitions are present in the $v'=1$ OODR spectra and appear at energies for which there are no corresponding lines in the $v'=0$ spectra. These new lines must be transitions to $v=0$ out of $v'=1$ and are thus signatures of $v=0$ Rydberg levels.

The potential-energy curves of all Rydberg states should be nearly identical because they are characteristic of the molecular-ion core, and the Rydberg electron should have only a small bonding or antibonding (shielding) effect on the core at intermediate-n^* values. The observed vibrational intervals, summarized in Table V, show this to be the case. The fundamental vibrational frequency of the molecular ion core, $\Delta G_{1/2}=T_1-T_0$, can be inferred from these data to be 683 ± 2 cm^{-1}. Because $\Delta G_{1/2}$ varies so little among the Rydberg states, we can use the measured values for a few states to assign all the vibrational levels observed in the $v'=0$ spectra.

Taking only the $v=0$ levels and requiring that quantum defects for each series be as constant as possible over the range for which we have spectroscopic data, Eq. (1) allows us to extrapolate from our data to calculate $E_{IP}=46\,998\pm 5$ cm^{-1}. Of course, none of the series actually have constant quantum defects. The uncertainty we report is an estimate of the range over which E_{IP} can be varied without introducing a significant net upward or downward trend into the full set of quantum defects which can be derived from our data. Our E_{IP} is considerably higher than the 5.50 ± 0.02-eV ($44\,358\pm 200$-cm^{-1})

value determined recently from the CaF^+ appearance potential in an electron-bombardment experiment [15]. We do not understand the reason for this discrepancy, especially as the results of Kitaev *et al.* are in agreement with earlier results obtained by Hildenbrand using the same technique [16]. But, in support of our determination of E_{IP}, it should be noted that we have observed well-behaved $v=0$ Rydberg states at energies well above the E_{IP} determined by the electron-bombardment experiments.

The molecular constants determined from our data are given in Tables II–IV. Standard forms of the $^2\Sigma^+$ and $^2\Pi$ effective Hamiltonians in Hund's case (a) basis were used. The matrix elements are given by Coxon [17] and by Kotlar *et al.* [18]. For $^2\Delta$ we used the effective Hamiltonian given by Brown, Cheung, and Merer [19]. We varied only the most significant terms in these effective Hamiltonians. Parameters which have energy effects too small to be measured from our data were either set to zero or held fixed at reasonable values. For the $^2\Sigma^+$ states, T_0, B, and the spin-rotation parameter γ were varied to fit the measured transition energies. For the $^2\Pi$ and $^2\Delta$ states, T_0, B, A, and the Λ-doubling parameters p and q were varied.

The measured spin-orbit, Λ-doubling, and spin-rotation parameter values support our groupings into Rydberg series and our assignments of vibrational progressions. Successive members of each Rydberg series exhibit the expected smooth variation in these parameters. Different vibrational levels of the same electronic state show nearly identical parameter values, as must be the case in the absence of vibrational perturbations if our vibrational assignments are correct.

The final columns in Tables II–IV list *nominal ns, np,* or *nd* parentage based solely on extrapolation of each series to a valence state whose mixed Ca^+ *nl* character

TABLE II. Molecular constants of newly observed $^2\Sigma^+$ Rydberg states of CaF. All energy units are cm^{-1}. 1 standard deviation (1σ) uncertainties in the least significant digit are given in parentheses.

n^*	v	T_v	B_v	γ	Nominal Ca^+ *nl*
4.183	0	40 725.11(8)	0.3751(2)		5*p*
4.18	2	42 091(5)[a]			5*p*
4.899	0	42 427(5)[a]	0.369(2)	+0.0188(5)	6*d*
5.184	0	42 915(5)[a]	0.375(1)	−0.0080(5)	6*p*
4.90	1	43 110.7(2)	0.365 96(3)	(+)0.0184(8)[b]	6*d*
5.551	0	43 437.3(2)	0.372 41(5)	(+)0.0023(17)[b]	8*s*
5.18	1	43 597.4(2)	0.373 98(2)	(−)0.0076(7)[b]	6*p*
4.90	2	43 792.1(2)			6*d*
5.880	0	43 824.1(2)	0.368 97(3)	(+)0.0163(12)[b]	7*d*
5.55	1	44 121.7(5)			8*s*
6.187	0	44 131.3(5)	0.378 91(2)	−0.0078(6)	7*p*
5.18	2	44 276.7(2)	0.370 2(1)	(−)0.0081(4)[b]	6*p*
6.549	0	44 438.9(2)	0.373 38(4)	+0.0035(3)	9*s*
5.87	1	44 505.2(5)	0.367 35(2)	(+)0.0152(9)[b]	7*d*
6.878	0	44 678.2(2)	0.368 10(1)	(+)0.0130(6)[b]	8*d*
5.55	2	44 799.8(5)			8*s*
6.19	1	44 820.3(5)			7*p*
7.189	0	44 874.80(2)	0.379 8(1)		8*p*
5.18	3	44 947(5)[a]			6*p*
7.546	0	45 070.57(3)	0.373 4(1)		10*s*
6.55	1	45 125(5)[a]			9*s*
5.88	2	45 181(5)[a]			7*d*
7.871	0	45 226.91(3)	0.364 3(1)		9*d*
8.188	0	45 361.19(6)	0.376 5(3)		9*p*
6.18	2	45 483.9(2)			7*p*
8.549	0	45 496.4(2)			11*s*
7.18	1	45 562.3(2)			8*p*
8.868	0	45 602.6(2)			10*d*
9.196	0	45 700.3(2)			10*p*
7.55	1	45 754.9(2)			10*s*

[a]The large estimated error is due to the incorporation of data from uncalibrated laser scans into the determination of this parameter.

[b]The sign of this constant could not be determined from the spectroscopic data from this state alone. The sign in parentheses is inferred from the observed signs of this parameter for other vibrational levels of the same electronic state or for other electronic states in the same Rydberg series.

TABLE III. Molecular constants of newly observed $^2\Pi$ Rydberg states of CaF. All energy units are cm^{-1}. 1σ uncertainties in the least significant digit are given in parentheses.

n^*	v	T_v	B_v	A	p	q	Nominal Ca^+ nl
3.98	1	40 716(5)[a]					6p
4.37	0	41 280(5)[a]					5d
4.37	1	41 957.1(2)	0.369(8)	3.6(2)			5d
4.973	0	42 561(5)[a]	0.371 2(5)	3.68(2)			7p
4.38	2	42 642(5)[a]	0.365(1)	3.61(2)			5d
5.360	0	43 178.0(2)	0.372 60(5)	1.95(3)	+0.006(4)	+0.002 11(5)	6d
4.97	1	43 242.3(2)	0.366 9(3)	3.81(1)			7p
5.36	1	43 865.3(2)	0.370 0(2)	1.87(3)	+0.002(4)	+0.001 60(4)	6d
5.975	0	43 923.8(2)	0.372 1(1)	2.10(5)	+0.003(4)	−0.000 72(7)	8p
6.353	0	44 278.9(2)	0.373 4(1)		−0.005(3)	+0.004 8(1)	7d
5.36	2	44 546.6(5)					6d
5.98	1	44 607.8(5)					8p
6.976	0	44 743.2(2)	0.370 8(1)		−0.003(3)	−0.001 40(6)	9p
7.31[b]	0	44 946.3(2)	0.371 6(3)		+0.018(5)	+0.008 3(1)	8d
6.39[b]	1	44 988.3(2)	0.372 4(1)			+0.003 9(1)	7d
7.977	0	45 273.54(2)	0.368 2(2)			−0.002 5(2)	10p
5.98	2	45 288(5)[a]					8p
8.342	0	45 421.20(6)	0.376 4(3)			+0.009 7(3)	9d
6.98	1	45 430.1(2)					9p
7.36	1	45 623.7(2)					8d
8.976	0	45 636.0(2)					11p
9.348	0	45 742.1(2)					10d
9.98	0	45 897.1(2)					12p

[a]The large estimated error is due to the incorporation of data from uncalibrated laser scans into the determination of this parameter.

[b]A strong $\Delta v = 1$ perturbation between these states results in $\sim$20-cm^{-1} shifts in their energies, extensive mixing of their wave functions, and interference effects in the transition intensities from $A\,^2\Pi$. These effects are discussed in Ref. [9] and an analysis will be presented in a future publication.

was calculated in the RMF model. Of course, l is not a good quantum number for an electronic state (especially a valence state) of a diatomic molecule. The ligand-field treatment has already shown that there is strong $p \sim d$ mixing in the lowest electronic states. Additional information about l mixing will be derived from our analysis of spin-orbit splittings.

IV. DISCUSSION

A. Quantum-defect determinations

The quantum-defect formalism [Eq. (1)] is useful because it defines a scaling parameter n^*, which allows the energies and other properties of all members of a Ryd-

TABLE IV. Molecular constants of observed $^2\Delta$ Rydberg states of CaF. All energy units are cm^{-1}. 1σ uncertainties in the least significant digit are given in parentheses.

n^*	v	T_v	B_v	A	p	q	Nominal Ca^+ nl
4.13	1	41 223(10)[a]	0.36(1)	1.13(3)			5d
4.13	2	41 921.1(2)	0.366(1)				5d
5.136	0	42 830(5)[a]	0.38(1)	0.56(3)			6d
5.13	1	43 517.8(2)	0.363(5)	0.30(9)			6d
6.135	0	44 082.4(2)	0.374(1)		$4(4)\times10^{-6}$	$-3(3)\times10^{-8}$	7d
5.13	2	44 195.5(2)	0.38(1)				6d
6.13	1	44 766.4(2)	0.371(1)	0.47(9)		$-3(2)\times10^{-7}$	7d
7.137	0	44 843.7(5)	0.374 10(5)		$-3(30)\times10^{-7}$	$-4(3)\times10^{-8}$	8d
8.134	0	45 339.3(2)	0.374 8(2)				9d
6.14	2	45 446.1(2)					7d
7.14	1	45 531.5(2)					8d
9.131	0	45 681.8(2)					10d

[a]The large estimated error is due to the incorporation of data from uncalibrated laser scans into the determination of this parameter.

TABLE V. Vibrational intervals of CaF Rydberg states. All energy units are cm^{-1}.

n^*	$^{2S+1}\Lambda$	$\Delta G_{1/2}$	$\Delta G_{3/2}$	$\Delta G_{5/2}$
4.89	$^2\Sigma^+$	684(5)	681.4(2)	
4.97	$^2\Pi$	681(5)		
5.14	$^2\Delta$	688(5)[a]	677.7(2)	
5.19	$^2\Sigma^+$	682(4)[a]	679.3(2)	671(5)[a]
5.36	$^2\Pi$	687.3(2)	681.3(2)	
5.55	$^2\Sigma^+$	684.4(5)	678.1(5)	
5.88	$^2\Sigma^+$	681.1(5)	676(5)[a]	
5.98	$^2\Pi$	684.0(5)	680(5)[a]	
6.14	$^2\Delta$	684.0(2)		
6.19	$^2\Sigma^+$	689.0(5)		
6.56	$^2\Sigma^+$	686(5)[a]		

[a]The large estimated error is due to the incorporation of data from uncalibrated laser scans into the determination of this parameter.

berg series to be predicted once those of one member are known. Thus the unique characteristics of each state are separated into the series-specific properties whose origins may be found in the inner lobes of the orbitals, and scaling relations which predict how those properties will vary with n^* within a series. Equation (1) provides an empirical definition of n^* for each Rydberg state based upon its observed energy. In the quantum-defect formalism, n^* is also defined by $n^*=n-\mu$, so Eq. (1) and the requirement that n be an integer determine μ to mod-1. Since a great deal is known about the lowest-energy states of CaF, there is some basis for defining n absolutely for each state and hence for fully defining μ. The expectation is that each Rydberg orbital contains inner lobes which recapitulate the form of the valence orbitals [8]. Both valence orbitals and the inner lobes of Rydberg orbitals are approximated by mixtures of the atomic orbitals of Ca^+ perturbed by a -1 point charge located at the F nucleus. The *nominal* value of n is then given by the Ca^+ orbital with which the molecular orbital correlates most strongly. For the *lowest-energy* members of each series, this dominant-nl orbital character can be taken from the RMF analysis. This then defines n for all the other members of the series.

Thus the $^2\Pi$ series which appears at $n^*=$integer $+0.98$ can be extrapolated to include the $A\,^2\Pi$ state and the $E\,^2\Pi$ state. The $A\,^2\Pi$ state has $n^*=1.88$, and, since it has been shown to have dominant Ca^+ $4p$ character, its quantum defect is taken as $\mu=4-1.88=2.12$ [2,20]. Since the quantum defect varies only slowly within a series, the (integer)$+0.02$ quantum defect for the higher members of this series must mean that, for them, $\mu=2.02$. The $^2\Pi$ series which appears at $n^*=$(integer)$+0.36$ has as its lowest members $C\,^2\Pi$ at $n^*=2.56$ and $F\,^2\Pi$ at $n^*=3.41$. These states have been assigned to Ca^+ $3d$ and $4d$ principal orbital parentage, respectively, giving $\mu=0.44$ and 0.61. For the higher members of this series $\mu=0.64$. The large difference in μ for $C\,^2\Pi$ compared with the other states in this series is due to the reverse polarization of the Ca^+-centered orbital toward fluorine [21], which causes a large destabilization (decrease of μ) due to overlap repulsion.

The terminus states of two of the three $^2\Sigma^+$ series are well known. $X\,^2\Sigma^+$ ($n^*=1.53,\mu=2.47$) is principally Ca^+ $4s$, and $B\,^2\Sigma^+$($n^*=1.98,\mu=1.02$) is principally Ca^+ $3d$. Both of these are polarized away from F^- [2,20]. The remaining $^2\Sigma^+$ terminus has recently been observed at $n^*=3.18$ [6]. While this state was not included in the RMF ligand-field calculation, by process of elimination this state is of nominal Ca^+ $4p$ parentage and thus has $\mu=0.82$.

The terminus of the lone $^2\Delta$ series is the $B'\,^2\Delta$ state recently observed by Barrow *et al.* [4] at $T_0=21\,518\ cm^{-1}$ ($n^*=2.075,\mu=0.925$). This state has Ca^+3d parentage. Thus $\mu=0.86$ for the $^2\Delta$ higher members of the series. With the observation of this $^2\Delta$ state and the $n^*=3.18$ $^2\Sigma^+$ state, our results indicate that the lowest member of each of the six core-penetrating Rydberg series, i.e., those derived from Ca^+ s, p, and d orbitals, is now known, and that *all low-lying $v=0$ states in the energy range spanned by Table I [22–27] have now been observed and correctly assigned,* except the $4d$ $^2\Delta$ state, whose predicted T_0 value is noted.

B. Spin-orbit interactions in Rydberg states

The next step beyond discussion of the $v=0$, rotationless term energies is analysis of the fine-structure interactions, starting with spin-orbit coupling in the $\Lambda\geq 1$ states. We have obtained sufficient rotationally resolved structure at low-J values to determine values of the spin-orbit interaction parameters for at least one vibrational level of four new $^2\Pi$ and three new $^2\Delta$ states. These states include at least two members from each of the $\Lambda\geq 1$ Rydberg series which we have identified.

Discussion of spin-orbit effects in molecular Rydberg states is fairly rare. Most previous experimental studies have dealt with molecules containing only lighter elements than calcium and/or such high-n states that spin-orbit splittings were undetectably small. The consequent lack of a clear paradigm for spin-orbit analysis in molecular Rydberg spectroscopy leads us to consider n and l scaling relationships from the analysis of atomic ion spectra as our starting point. We are also guided toward atomic concepts by the success of the atomic ion-in-molecule model in accounting for many features of the lowest-lying states [2,3] and the expectation that there will be some connection between that model and our eventually understanding of the Rydberg states.

In a simple monopole Coulomb field the spin-orbit constant for a single electron in a hydrogenic orbital with principal quantum number n and angular momentum quantum number l is given by

$$\zeta_{nl}=\frac{R\alpha^2Z^4}{n^3l(l+\frac{1}{2})(l+1)}\ , \tag{2}$$

where R is the Rydberg constant, α is the fine-structure constant ($R\alpha^2=5.8437\ cm^{-1}$), and Ze is the charge of the monopole (e is the electron charge) [28]. For a non-point charge but still spherical central field, such as that of an atom or ion with closed-shell core electrons, the

spin-orbit constant can be described empirically by a modification of Eq. (2) originally proposed by Landé [29]. With the symbols changed for clarity, this gives the spin-orbit constant as

$$\zeta_{nl}=\frac{R\alpha^2 Z_o^2 Z_i^2}{n^{*3} l(l+\frac{1}{2})(l+1)} \tag{3}$$

where n is now replaced by n^* $(n-\mu)$, Z_o (Z outer) is the charge of the bare core (as sampled at $r=\infty$), and Z_i (Z inner) may be considered to be the *effective* nuclear charge as sampled by Rydberg orbitals which extend inside the region occupied by the filled core orbitals [28,29]. In this formulation, the effects of penetration of the extended core by the Rydberg orbital are accommodated in two parameters Z_i and μ.

Because of the $\sim r^{-3}$ radial dependence of the spin-orbit operator, the dominant part of ζ_{nl} accumulates upon integration over the innermost lobe of the nl orbital. The orbital contraction implied by the positive quantum defect, which is characteristic of core-penetrating orbitals, affects ζ_{nl} in two ways: an increased amplitude in the innermost lobe, as reflected by μ in n^* of Eq. (3), and an increased Z as sampled by this inner lobe as reflected by Z_i. Since, aside from an $n^{*-3/2}$ scaling of its amplitude, the shape of the innermost lobe of a Rydberg orbital is independent of n along a Rydberg series, one expects the scaling of ζ_{nl} along each series to be given by an n-independent but l-dependent value of Z_i.

Calculation of Z_i values from Ca^+ atomic data [30] using Eq. (3) produces results which are consistent with this expectation. The Z_i value for each Ca^+ Rydberg state is always greater than the $+2$ charge of the ion core (Z_o) and is nearly constant within each series. The results are summarized in Tables VI and VII. The $np\ ^2P$ series shows a Z_i of 17.19 ± 0.04 up to $6p$ and the $nd\ ^2D$ series shows a Z_i of 13.7 ± 0.2 up to $10d$. The effective core penetration indicated by Z_i is clearly greater in the np series than in the nd series, as one would also expect from the larger quantum defect of the np series (np, $\mu=1.5$; nd, $\mu=0.6$).

Our initial premise is that the spin-orbit coupling constants of molecular Rydberg states may be treated in the same general manner as atomic Rydberg states. CaF is a particularly simple case since it is a one-electron system with a closed-shell core. We adapt Eq. (3) directly by assuming the same formula for A_{SO} as for ζ_{nl}, giving

TABLE VI. Spin-orbit parameters and effective core charges for states in the Ca^+ $np\ ^2P$ Rydberg series. Data from Ref. [30].

n	n^*	ζ_{nl} (cm^{-1})	Z_i[a]	$Z_i(l)$[b]
4	2.49	148.59	17.16	9.91
5	3.53	52.17	17.16	9.91
6	4.55	24.55	17.23	9.94

[a]Calculated using Eq. (3) with $Z_o=2$ and $l=1$.
[b]$Z_i(l)=Z_i[l(l+1/2)(l+1)]^{-1/2}$.

TABLE VII. Spin-orbit parameters and effective core charges for states in the Ca^+ $nd\ ^2D$ Rydberg series. Data from Ref. [30].

n	n^*	ζ_{nl} (cm^{-1})	Z_i[a]	$Z_i(l)$[b]
3	2.31	24.28	13.86	3.58
4	3.36	7.684	13.68	3.53
5	4.37	3.48	13.65	3.52
6	5.37	1.852	13.57	3.50
7	6.37	1.104	13.53	3.49
8	7.37	0.715	13.56	3.50

[a]Calculated using Eq. (3) with $Z_o=2$ and $l=2$.
[b]$Z_i(l)=Z_i[l(l+1/2)(l+1)]^{-1/2}$.

$$A_{SO}=\frac{R\alpha^2 Z_o^2 Z_i^2}{n^{*3} l(l+\frac{1}{2})(l+1)}=\frac{5.8437 Z_o^2 Z_i^2}{n^{*3} l(l+\frac{1}{2})(l+1)}\ \mathrm{cm}^{-1}. \tag{4}$$

In this equation Z_o is the charge of the molecular ion core, n^* is derived from Eq. (1), and A_{SO} is measured. We take Z_o to be $+1$ initially, an assumption which we will later examine in more detail. This leaves Z_i and l to be determined.

The value of Z_i for each molecular Rydberg state will be greater than the $+1$ charge of the CaF^+ molecular ion core to the extent that the inner lobes of the Rydberg orbital penetrate into the CaF^+ core. We expect Z_i to be constant within a series, as it is in the atomic case, and for Z_i to have different characteristic values for each Rydberg series due to their different degrees of core penetration.

However, Z_i cannot be calculated directly because l is not defined in the nonspherical molecular case. In Eq. (4), l must be treated as an effective parameter which expresses the effect of l mixing on the spin-orbit constant. The overall effect of core penetration and l mixing on A_{SO} will be shared between Z_i and the terms in l in the denominator. Since we cannot determine both Z_i and an effective value for l from Eq. (4) alone, we choose to combine the Z_i and the l-dependent terms into a single empirical parameter which we define as

$$Z_i(l)\equiv\frac{Z_i}{[l(l+\frac{1}{2})(l+1)]^{1/2}}=\left[\frac{A_{SO}n^{*3}}{5.84Z_o^2}\right]^{1/2}. \tag{5}$$

Equation (4) then becomes

$$A_{SO}=\frac{5.8437 Z_o^2[Z_i(l)]^2}{n^{*3}}\ \mathrm{cm}^{-1}. \tag{6}$$

As expected, Eq. (6) leads to n-independent values of $Z_i(l)$ when applied to the $^2\Pi$ and $^2\Delta$ Rydberg series which we have observed. The results are given in Tables VIII–X.

We expect the Ca^{2+} center in the molecular core to dominate the core-penetration-dependent effects in the Rydberg states because we expect that the inner lobes of these orbitals are identical to those of the calcium-centered valence precursor states analyzed by RMF. To

TABLE VIII. Spin-orbit parameters and effective core charges for states in the CaF $\mu=2.02$ $^2\Pi$ Rydberg series, from data reported in Tables I and II. Uncertainties (1σ) are given in parentheses.

n^*	A (cm^{-1})	Z_i[a]	$Z_i(l)$[b] ($Z_o=1.00$)	($Z_o=1.08$)
1.90 A	71.45	15.87	9.16	8.48
2.96 E'	16.9	15.00	8.66	8.00
4.98	3.68(2)	15.33(6)	8.85(3)	8.19(3)
5.98	2.10(5)	15.17(20)	8.76(10)	8.11(10)

[a]Calculated using Eq. (4) with $Z_o=1$ and $l=1$.
[b]Calculated using Eq. (6) with the Z_o values indicated.

TABLE X. Spin-orbit parameters and effective core charges for states in the CaF $\mu=0.87$ $^2\Delta$ Rydberg series, from data reported in Tables I and IV. Uncertainties (1σ) are given in parentheses.

n^*	A (cm^{-1})	$Z_i(l=2)$[a]	$Z_i(l)$[b] ($Z_o=1.00$)	($Z_o=1.08$)
2.08	12.398	16.9	4.34	4.02
4.13 ($v=1$)	1.13(3)	14.3(2)	3.69(5)	3.42(5)
5.136	0.56(3)	13.9(4)	3.60(10)	3.33(9)
6.135	0.47(9)	17(2)	4.3(4)	4.0(4)

[a]Calculated using Eq. (4) with $Z_o=1$ and $l=2$.
[b]Calculated using Eq. (6) with the Z_o values indicated.

test this expectation we compare properties of the CaF molecular and the Ca^+ atomic Rydberg series, both of which are built upon a Ca^{2+} core. Values for $Z_i(l)$ for the Ca^+ atomic series are calculated and listed in Tables VI and VII to make this comparison possible.

Two aspects of the spin-orbit behavior of the CaF $^2\Pi$ series contrast with the Ca^+ *np* and *nd* Rydberg series upon examination of the $Z_i(l)$ values derived from Eq. (6). First, the asymptotic values of $Z_i(l)$ for the two molecular $^2\Pi$ Rydberg series are much less different from each other than are those of the Ca^+*np* and *nd* series. CaF shows asymptotic series values, as determined by averaging all the values that could be measured from states above $n^*=4$ in a given series, of $Z_i(l)=8.8\pm0.3$ for the $\mu=2.02$ $^2\Pi$ series and $Z_i(l)=7.1\pm0.1$ for the $\mu=0.64$ $^2\Pi$ series, while Ca^+ by comparison shows $Z_i(l)=9.92\pm0.02$ for the *np* series and $Z_i(l)=3.52\pm0.06$ for the *nd* series. Near the Ca^{2+} ion in the molecular core we expect that the Rydberg orbitals of the two $^2\Pi$ series can be expanded solely in terms of basis functions which are members of the Ca^+ *np* and *nd* Rydberg series. The reasoning is that both $^2\Pi$ series are known to penetrate the Ca^{2+} core because they show large spin-orbit interactions and large quantum defects, and the only Ca^+ basis functions which penetrate the Ca^{2+} core and have $l>0$ are the members of the *np* and *nd* series. Of course it is possible that other series may be mixed through interaction terms which are not dependent upon Ca^+ core penetration, but the effect of these interactions on A_{SO} is expected to be negligible in comparison with core-penetration effects for the states discussed here. We choose to ignore such interactions. The fact that the values of $Z_i(l)$ for both CaF $^2\Pi$ series are intermediate between the values of $Z_i(l)$ for the Ca^+ *np* and *nd* series supports the conclusion of strong $p\sim d$ mixing in these two molecular $^2\Pi$ series.

The second observation about the $^2\Pi$ molecular series is that the average of their two asymptotic $Z_i(l)$ values is significantly *larger* than the corresponding average of the atomic *np* and *nd* series. This departure from trace invariance suggests that a molecular property other than $p\sim d$ mixing and Ca^{2+} core penetration affects $Z_i(l)$. Further refinement of the empirical model is necessary to isolate core penetration from this additional effect. Our modification is to retain the form of Eq. (4), but to allow Z_o to vary instead of holding it fixed at $+1$. To understand the rationale for adjusting Z_o, let us divide the space in which the electron moves into three regions as shown in Fig. 1. Core penetration for CaF may be thought of as really two effects, penetration into the spherical Ca^{2+} atomic ion core, or region III in Fig. 1, and penetration into the portion of the $(CaF)^+$ molecular ion core exclusive of the Ca^{2+} atomic ion, or Region II in Fig. 1. It is only the former type of core penetration that leads to contributions to A_{SO}, with the exception of those low-lying states which are strongly polarized toward the F^- and have some contribution from the fluorine nucleus. Thus only the Ca^{2+} penetration should be incor-

TABLE IX. Spin-orbit parameters and effective core charges for states in the CaF $\mu=0.64$ $^2\Pi$ Rydberg series, from data reported in Tables I and II. Uncertainties (1σ) are given in parentheses.

n^*	A (cm^{-1})	Z_i[a]	$Z_i(l)$[b] ($Z_o=1.00$)	($Z_o=1.08$)
2.56	29.24	35.35	9.13	8.45
3.418	9.184	30.67	7.92	7.34
4.37 ($v=1$)	3.6(2)	27.8(8)	7.17(20)	6.64(18)
5.36	1.95(2)	27.8(2)	7.17(5)	6.64(5)

[a]Calculated using Eq. (4) with $Z_o=1$ and $l=2$.
[b]Calculated using Eq. (6) with the Z_o values indicated.

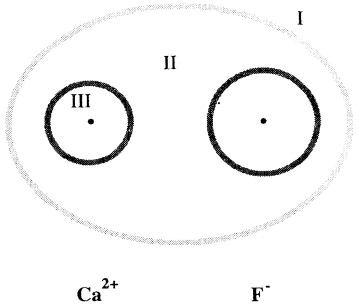

FIG. 1. Schematic representation of $(CaF)^+$ indicating the spatial regions in which the environments of the Rydberg electron are qualitatively different.

porated into $Z_i(l)$ if this parameter is to be used to compare the molecular spin-orbit interactions with those of Ca^+ states. This falling-onto-Ca^{2+} type of core penetration can be isolated by adjusting Z_o.

The adjusted Z_o expresses the deviation from complete shielding of the Rydberg electron from the Ca^{2+} core by the F^- ion in much the same way that Z_i expresses the incomplete shielding of the electron from the calcium nucleus by the Ca^{2+} core electrons. The appropriate value of Z_o will be less than the $+2$ charge of the bare Ca^{2+} ion because of this F^- shielding, and it will be greater than the formal $+1$ charge of the molecular ion core to the extent that the shielding is incomplete. Fundamentally, both the F^- ion and the electrons of Ca^{2+} contribute to the screening of the Rydberg electron from the calcium nucleus, thus moderating the spin-orbit interaction. In seeking to frame the discussion of molecular Rydberg states in terms of Ca^+ Rydberg states, the additional adjustable parameter (Z_o) is necessary to remove the difference in screening experienced by the molecular Rydberg electron so that the remainder of the problem allows a direct comparison with the atomic case.

The approach to adjusting Z_o is based on the expectation that if all interactions except $p\sim d$ mixing are removed from $Z_i(l)$, and if only $Ca^+ np$ and nd series mix to form the $^2\Pi$ series, then the two molecular series will have the same average value for this reduced spin-orbit interaction parameter as the Ca^+ parent states. A new Z_o is determined by requiring that the values of $Z_i(l)$ for the two $^2\Pi$ series calculated using the adjusted Z_o in Eq. (6) sum in quadrature to the same total as the values for $Z_i(l)$ for the $Ca^+ np$ and nd series. Imposing this requirement, we obtain an adjusted Z_o value of 1.08 for the $^2\Pi$ series.

Substituting 1.08 for Z_o in Eq. (6), we recalculate values of $Z_i(l)$ for each of the molecular Rydberg states. The results are shown in the final columns of Tables VIII–X. The magnitude of Ca^+ $p\sim d$ series mixing in the $^2\Pi$ series can then be derived by using these new values for $Z_i(l)$ and the assumption that the contribution of np and nd Ca^+ series to a $p\sim d$ mixed molecular series is of the form

$$[Z_i^{\mathrm{CaF}}(l)]^2=\alpha^2[Z_i^{\mathrm{Ca}^+}(p)]^2+\beta^2[Z_i^{\mathrm{Ca}^+}(d)]^2\ ,\qquad \alpha^2+\beta^2=1\ . \tag{7}$$

Here α and β are mixing coefficients in the expansion of the molecular $^2\Pi$ series in the region of the Ca^{2+} ion in terms of the Ca^+ p and d series. The squares of these coefficients give the fractional p and d character in the molecular series. We determine that the $\mu=2.02$ $^2\Pi$ series is 63% np ($\alpha^2=0.63$) and 37% nd ($\beta^2=0.37$), while the $\mu=0.64$ $^2\Pi$ series is 37% np and 63% nd. These mixing coefficients are generalized *series* mixing coefficients, not mixing coefficients for individual Ca^+ basis states. We are not implying that each molecular $^2\Pi$ Rydberg state is a mixture of a single $Ca^+ np$ state and a single $Ca^+ nd$ state. By not considering the mixing of individual basis states, this treatment sidesteps the important issue of $nl\sim(n+1)l$ mixing of Ca^+ states for the moment.

For the lone observed $^2\Delta$ series, the $Z_i(l)$ values in the final column of Table VIII were recalculated using the adjusted value of $Z_o=1.08$ determined from the $^2\Pi$ series alone. To within the precision of its determination, the recalculated asymptotic value of $Z_i(l)=3.5\pm0.2$ for the $^2\Delta$ series matches that for the $Ca^+ nd$ series [$Z_i(l)=3.52\pm0.06$] exactly. Recall that this was not true of the recalculated values of $Z_i(l)$ for either of the $^2\Pi$ series, both of which have asymptotic values of $Z_i(l)$ between those of Ca^+ np and nd states. The close correspondence between atomic and molecular parameters for the $^2\Delta$ series is reasonable because the $^2\Delta$ states will be nearly pure nd at low J. There are no Ca^+ states of higher l which are also core penetrating from which the $^2\Delta$ series could acquire mixed-l character. This agreement between the atomic and molecular values of $Z_i(l)$ lends credibility to the model proposed here.

C. Spin-orbit interactions in valence states

Thus far we have excluded the lowest Rydberg and valence states from our discussion because their spin-orbit constants deviate from those predicted by scaling relations using the asymptotic scaling coefficients determined from the intermediate Rydberg states. If we set $Z_i(l)$ at the asymptotic series value, and use $Z_o=1.08$ and the measured n^* values in Eq. (6), we can calculate extrapolated spin-orbit constants for the A $^2\Pi$ and C $^2\Pi$ states. We find that the experimental A_{SO}'s are significantly larger than these extrapolated values. The A state, in addition to a larger experimental A_{SO}, also has a larger experimental quantum defect ($\mu=2.10$) than the series average of $\mu=2.02$. These deviations from the behavior of the higher members of the series are consistent with each other because one would expect that greater *molecular core* penetration (larger μ) will be accompanied by greater *Ca^{2+} core* penetration (larger Z_i) resulting in a larger spin-orbit splitting. The deviation from the limit observed for higher series members could be due to reduced shielding by F^- in this lowest (most compact) "Rydberg" orbital, with the result that this orbital in the A $^2\Pi$ state is more Ca^{2+} centered than in higher members of the series. One could make the same argument by fixing $Z_i(l)$ at the series limit and using Eq. (6) to adjust Z_o to fit the experimental spin-orbit values. The result for the A $^2\Pi$ state, $Z_o=1.12$, is larger than that for the series as a whole, indicating greater molecular core penetration and stronger interaction with the Ca^{2+} ion.

The RMF ligand-field calculation *overestimated* the spin-orbit splitting in the A $^2\Pi$ state by 20%. This deviation is in the opposite direction to the 9% underestimate based on the extrapolation from the higher members of the $\mu=2.02$ $^2\Pi$ Rydberg series. The reason for this difference between the ligand field and Rydberg estimates of A_{SO} in the A $^2\Pi$ state is that the ligand-field model implicitly assumes $Z_o=2$ by using ζ_{n^*p} and ζ_{n^*d} values from the Ca^+ ion, whereas the Rydberg model implicitly assumes $Z_o=1$. Neither zero-order picture is correct for the A $^2\Pi$ state.

The ligand-field model attempts to deal with repulsion

of the Ca^{2+}-centered electron by a -1 point-charge ligand by including both $nl \sim (n+1)l$ and $nl \sim n(l+1)$ orbital mixing. Both types of mixing minimize repulsion of the Ca^{2+}-centered electron by the F^- ligand, the former by increasing the size of the orbital and the latter (in the case of the $A\,^2\Pi$ state but not the oppositely "reverse" polarized $C\,^2\Pi$ state) by polarizing the expanded orbital into the region on the opposite side of the Ca^{2+} ion from the F^- ligand. Although the $4p$, $5p$, $3d$, and $4d$ orbital mixing coefficients were specified in the eigenvectors of the zero-adjustable-parameter ligand-field model, RMF did not include spin-orbit cross terms of the form $\langle nl|H^{SO}|n+1l\rangle$ in the spin-orbit calculation because of the expected sensitivity to details of the inner lobes of the very crude atomic orbitals which were used.

Subsequently, Pitzer calculated such $nl \sim (n+1)l$ spin-orbit matrix elements for Ca^+ and found [31], to an excellent approximation, that

$$\langle nl|\mathbf{H}^{SO}|n'l\rangle \propto (-1)^{(n-n')}[\zeta_{nl}\zeta_{n'l}]^{1/2} \tag{8}$$

with the phase choice that the outermost lobe of the radial wave function R_{nl} is always positive. For this phase choice, the $\langle nl|r^2|n+1l\rangle$ ligand-field matrix element responsible for the $nl \sim (n+1)l$ orbital mixing is always positive, because this matrix element is dominated by the outermost lobe of the atomic Ca^+ wave functions. As a result, when the spin-orbit cross term is included in the RMF model, the predicted ligand-field value of A_{SO} for the lowest member of each Rydberg series will be significantly decreased. The predicted value of A_{SO} for the second member of each series will be slightly increased due to canceling effects from the $(n+1)l \sim nl$ and $(n+1)l \sim (n+2)l$ interactions.

Consideration of the $nl \sim (n+1)l$ orbital mixing effect is the major adjustment which must be made to the ligand-field model to compensate for a too-large zero-order value of $Z_o \approx 2$. The Rydberg model, on the other hand, is based on a too-small value of $Z_o \approx 1$ for the low-lying states, in which the Rydberg orbital starts to collapse onto the Ca^{2+} atomic ion rather than the $(CaF)^+$ molecular ion. Similar $n^*l \sim (n^* \pm 1)l$ orbital mixing effects must occur in the Rydberg model in order to produce the necessary extra contraction of the lowest-n^* orbital of each series. This means that A_{SO} for the first two members of each Rydberg series will also be affected by $\langle n^*l|r^2|(n^* \pm 1)l\rangle$ cross terms. Neglect of the cross terms will lead to discrepancies of opposite sign to those of the RMF model. Thus extrapolation from the spin-orbit scaling of the states at higher energy will lead, respectively, to a large underestimate and a small overestimate for the first and second members of each series. These effects are observed in the spin-orbit constants of the $A\,^2\Pi$ and $E'\,^2\Pi$ states.

The $C\,^2\Pi$ state also has properties which deviate from those common to higher members of its Rydberg series ($\mu = 0.64$), but these deviations are somewhat different from those of the $A\,^2\Pi$ state. Like the $A\,^2\Pi$ state, the $C\,^2\Pi$ state has a *larger* experimental A_{SO} than what one predicts by extrapolating from the higher members of the series, indicating greater penetration of the Ca^{2+} core. Its quantum defect, however, is *smaller* than the high-n^* limiting value of the series, which would seem to suggest less penetration of the molecular core. A different explanation from that used for the $A\,^2\Pi$ state must be developed which explains this apparent inconsistency.

The $C\,^2\Pi$ state is unusual in that the orbital occupied by the valence electron is polarized toward F^- [21]. This reverse polarization provides the key to the resulting spin-orbit and quantum defect anomalies in the $C\,^2\Pi$ state of all Ca, Sr, and Ba monohalides [2,3]. The $p \sim d$ mixing induced by the X^- ligand results in an $|a\pi\rangle^0$ orbital polarized out the back side of the M^+ ion in the $A\,^2\Pi$ state (away from X^-) and a $|c\pi\rangle^0$ orbital polarized out the front side of the M^+ in the $C\,^2\Pi$ state. The back-side polarization of $|a\pi\rangle^0$ makes a correction for overlap with X^- orbitals unnecessary, because the overlap integral $\langle a\pi(M^+)|p\pi(X^-)\rangle$ is very small. The front-side polarization of $|c\pi\rangle^0$ demands an overlap correction (Schmidt orthogonalization)

$$|c\pi\rangle = [1 - S^2_{c\pi,p\pi}]^{-1/2}[|c\pi\rangle^0 - S_{c\pi,p\pi}|p\pi\rangle^0] , \tag{9}$$

where

$$S_{c\pi,p\pi} = {}^0\langle c\pi(M^+)|p\pi(X^-)\rangle^0 \tag{10}$$

and $S_{c\pi,p\pi}$ is evaluated at R_e. The spin-orbit constant for the $C\,^1\Pi$ state is then given by

$$\langle c\pi|Al_z|c\pi\rangle = \frac{1}{1 - S^2_{c\pi,p\pi}}[A^0_{c\pi} + S^2_{c\pi,p\pi}\zeta_{np}(X^-)] , \tag{11}$$

where $A^0_{c\pi}$ is the crude Rydberg-series extrapolation neglecting overlap and $\zeta_{np}(X^-)$ is the estimated spin-orbit coupling constant for the filled np orbital of the X^- ligand. $\zeta_{np}(X^-)$ values for F^-, Cl^-, and Br^- are estimated from $\zeta_{np}(X^-) \approx \zeta_{np}(X) - \{\zeta_{np}(X^+) - \zeta_{np}(X)\}$, giving 211, 510, and 2354 cm^{-1}, respectively [32]. For the CaF $C\,^2\Pi$ state, the increase in A_{SO} relative to the Rydberg series extrapolation $A^0_{c\pi}$ is due to two factors, $1 - S^2 < 1$, and $\zeta_{2p}(F^-) \approx 211$ $cm^{-1} > \zeta_{4p}(Ca^+)$ ($= 149$ cm^{-1}) and $\zeta_{3d}(Ca^+)$ ($= 24$ cm^{-1}). The value for $S_{c\pi,p\pi}$ obtained from Eq. (11) using $A_{c\pi} = 29$ cm^{-1}, $A^0_{c\pi} = 18$ cm^{-1} [Eq. (4) with $Z_o = 1.08$, $l = 2$, $Z_i = 27.7$, and $n^* = 2.56$], and $\zeta_{2p}(F^-) = 211$ cm^{-1} is $S_{c\pi,p\pi} = 0.21$, a plausible value. As n^* increases along a Rydberg series, this overlap correction to A_{SO} will decrease, although it will never vanish entirely.

The above discussion of the $A\,^2\Pi$ state has already shown that the terminus states are expected to differ from the rest of their respective series in that they will exhibit the effects of unique $n^*l \sim (n^*+1)l$ orbital mixing. For the $A\,^2\Pi$ state and the $B'\,^2\Delta$ state the observed deviation in the spin-orbit scaling parameter $Z_i(l)$ at the series terminus can be explained as being due to an increase in the effective core charge which occurs when the Rydberg orbital partially collapses onto the Ca^{2+} ion. The $C\,^2\Pi$ state is subject to the same effect, but with the complication unique to the $C\,^2\Pi$ state that there is a strong interplay between the orbital contraction and the large overlap with the F^- $2p$ orbitals. In the $C\,^2\Pi$ series terminus

state the Rydberg orbital also tries to collapse onto the F^- ion. For the $C\,^2\Pi$ state, where $S_{c\pi,p\pi}$ is large and cannot be ignored, this produces a much larger deviation of the spin-orbit scaling factor from the series limit than is observed in the other terminus states, where overlap can effectively be neglected. It also produces a decrease in the quantum defect, where an increase is observed for the other series terminus states.

D. Λ doubling

The measured values of the Λ doubling (p and q) and spin-rotation (γ) parameters for the $^2\Pi$ and $^2\Sigma^+$ Rydberg states (Tables II and III) have proven to be useful as empirical, series-identification diagnostics. On the basis of naive expectations of smooth intraseries variation and large interseries differences, these parameter values confirm the original, energy-scaling-based arrangement of the observed states into series. The γ parameters are roughly constant within each $^2\Sigma^+$ series and significantly different between series. The q parameter value increases with n^* for states in both of the $^2\Pi$ series, and $^2\Pi$ states with similar n^* values, but belonging to different series, differ significantly in the magnitudes and signs of their q parameters.

In this section we extend the analysis of these l-uncoupling interactions by identifying and interpreting the scaling of the observed parameter values. As with the spin-orbit constants, quantitative scaling relationships can be developed which describe the observed parameter values in terms of a product of a series-specific coefficient, which is sensitive to the nl atomic orbital parentage and to interseries interactions, and a function of n^* which is the same for all states. We then attempt to calculate the parameter values by assuming dominant two-state interactions. We get some insight into the dominant perturbations from this modeling, but our basic conclusion is that this simplified approach works well for the valence states but fails as one moves up in n^*. We explain why the dominant 2×2 interaction model fails at high n^* and discuss how to model the higher-n^* Rydberg supercomplexes.

The scaling of p, q, and γ can be anticipated based on the definitions of these parameters in terms of perturbation matrix elements between Born-Oppenheimer electronic states. Considering only rotational and spin-orbit Σ-Π perturbations and assuming identical potential curves for all interacting states, p and q are given by [17]

$$p_i=\sum_j \frac{2\langle {}^2\Pi_i|A(r)L_+|{}^2\Sigma_j^+\rangle\langle {}^2\Pi_i|B(r)L_+|{}^2\Sigma_j^+\rangle}{E_{\Pi_i}-E_{\Sigma_j}}$$

$$=\sum_j \frac{a_{+ij}b_{ij}B(r)}{\Delta E(\Pi\Sigma)_{ij}} \tag{12}$$

and

$$q_i=\sum_j \frac{2\langle {}^2\Pi_i|B(r)L_+|{}^2\Sigma_j^+\rangle^2}{E_{\Pi_i}-E_{\Sigma_j}}=\sum_j \frac{b_{ij}^2B(r)^2}{\Delta E(\Sigma\Pi)_{ij}} \tag{13}$$

and γ is given by

$$\gamma_i=-\sum_j \frac{2\langle {}^2\Sigma_i^+|A(r)L_+|{}^2\Pi_j\rangle\langle {}^2\Sigma_i^+|B(r)L_+|{}^2\Pi_j\rangle}{E_{\Sigma_i}-E_{\Pi_j}}$$

$$=-\sum_j \frac{a_{+ij}b_{ij}B(r)}{\Delta E(\Pi\Sigma)_{ij}} \tag{14}$$

where i indexes the state for which the parameter is measured and j indexes all possible perturbing states. $A(r)$ and $B(r)$ are the spin-orbit and rotational constants and a_+ and b are the one-electron matrix elements $a_+=\langle\pi|\hat{a}l_+|\sigma\rangle$ and $b=\langle\pi|l_+|\sigma\rangle$, whose substitution is valid for the present case because there is only one electron outside of the closed-shell, molecular ion core [32]. The expected scaling of p, q, and γ within individual Rydberg series can be determined by the scaling of the components on the right-hand sides of Eqs. (12)–(14).

If the quantum defects are constant throughout each Rydberg series, the scaling of the energy difference between two Rydberg states whose n^* values differ by $\delta=n^{*\prime}-n^*$ approaches a limit of

$$\Delta E=2R\delta/n^{*3} \tag{15}$$

as n^* increases. All interseries energy differences between states which belong to the same ion core vibrational level obey this scaling relation, distinguished only by the value of δ. Thus all of the energy denominators in Eqs. (12)–(14) follow the same $\Delta E(\Pi,\Sigma)_{ij}\propto n^{*-3}$ scaling law.

The scaling of the matrix elements in the Eqs. (12)–(14) numerators can be deduced from the forms of their operators. Like the diagonal spin-orbit matrix elements discussed in Sec. IV B, the off-diagonal matrix elements containing $A(r)$ will scale as $1/n^{*3}$. Matrix elements of L_+ will be independent of n^* because L_+ acts only on the angular parts and not on the radial parts of the wave functions. And the matrix elements of $B(r)$ are constant because the molecular ion-core rotation-vibration parameters are essentially the same in all of the Rydberg states beyond the lowest few members of each series. Combining the scaling of the terms in the numerators with the derived $1/n^{*3}$ scaling of the energy denominators, the expectation is that p will be independent of n^*, because both the numerator and the denominator scale as $1/n^{*3}$, and that q will scale as n^{*3}, because the numerator is independent of n^*. And γ, like p, should be independent of n^*. The parameter values extracted from our spectroscopic data confirm that these scaling relations approximate the actual behavior of the experimental q and γ values quite well. We have been unable to determine sufficiently accurate values of p to evaluate the scaling behavior of this parameter.

Note that Eqs. (12)–(14) are written as sums over perturbing electronic states. Several Rydberg states of appropriate Λ are close enough in energy to perturb each $^2\Sigma^+$ and $^2\Pi$ state, so several possible interseries perturbations must be considered as potential contributors to the observed p, q, and γ values. We fully expect that the contributions from several perturbing states will eventually be found to be significant. However, in a simple attempt to identify the dominant perturber(s) of each state we be-

gin with the working hypothesis that the Λ doublings or spin-rotation splittings of each $^2\Pi$ or $^2\Sigma^+$ state can be analyzed as being due primarily to interactions with one other Rydberg state. Under this overly simple *unique-perturber* hypothesis, a positive γ or a negative q is characteristic of a dominant perturbation by a state at higher energy. Thus each member of the $\mu=1.12$ $^2\Sigma^+$ series is inferred to interact primarily with a $^2\Pi$ state at high energy, and each member of the $\mu=0.81$ $^2\Sigma^+$ series is inferred to interact primarily with a $^2\Pi$ state at lower energy. Each member of the $\mu=0.64$ $^2\Pi$ series is inferred to interact primarily with a $^2\Sigma^+$ state at lower energy, and each member of the $\mu=2.02$ $^2\Pi$ series is inferred to interact primarily with a $^2\Sigma^+$ state at higher energy. The γ value for the $\mu=2.45$ $^2\Sigma^+$ series, while positive, is smaller than the γ values of the other two $^2\Sigma^+$ series. This indicates, within the present hypothesis, that members of the $\mu=2.45$ series interact least strongly with nearby $^2\Pi$ states.

Consider the subset of intermediate energy Rydberg states displayed in Fig. 2 as representative of all of the observed Rydberg states. Of this group of states, mutual proximity in energy suggests that interaction among the members of the group of states which lie between $n^*=5.5$ and 6.5 might be analyzed by neglecting perturbations from outside the group. The $^2\Sigma^+$ and $^2\Pi$ states which are observed to have the largest interaction parameters are in the center of the group, giving the best chance of accounting for their interaction parameters without going outside the group, and the signs of the interaction parameters of the extreme states in the group,

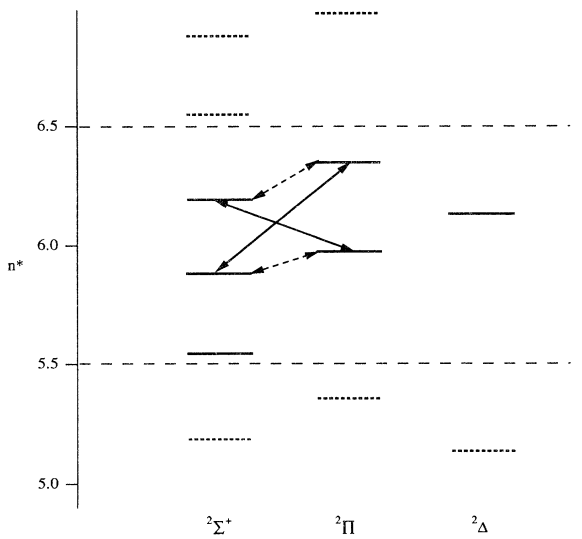

FIG. 2. Energies (plotted as n^*) of intermediate core-penetrating Rydberg states of CaF. The states which are in the mutually interacting group discussed in the text are those in the energy region between the long-dashed lines. The states just outside this group are shown as short-dashed lines. Pairwise interactions deduced from the Λ-doubling and spin-rotation constants are indicated by arrows, with the weaker interactions shown as dashed arrows.

with the exception of the 5.55 $^2\Sigma^+$ state (which has the smallest γ value of the three $^2\Sigma^+$ states), indicate primary interactions with states internal to the $5.5<n^*<6.5$ group rather than external to it. Assuming, for simplicity, that the unique-perturber model is approximately valid within this grouping, the signs of the interaction parameters q and γ imply the perturbation pairings indicated by the solid arrows in Fig. 2.

The relative magnitudes of the q and γ parameters also support the $^2\Pi(n^*=6.36)\sim{}^2\Sigma^+(n^*=5.88)$ and $^2\Pi(n^*=5.98)\sim{}^2\Sigma^+(n^*=6.19)$ dominant interaction pairings. Of the two $^2\Sigma^+$ states considered so far, the one with the smaller γ value has been paired with the $^2\Pi$ state with the smaller q value, and the one with the larger γ value has been paired with the $^2\Pi$ state with the larger q value. The best test of the unique-perturber model for $^2\Sigma^+$-$^2\Pi$ interacting pairs is the equivalence of the γ for the $^2\Sigma^+$ state to p for the $^2\Pi$ state. Because we have not been able to determine p for any of the $^2\Pi$ states, we are unable to proceed with the evaluation of the unique-perturber hypothesis for this set of states beyond saying that *if* the hypothesis were valid, then the pairings must be as indicated.

The dominant $^2\Sigma^+\sim{}^2\Pi$ interactions that we have tentatively identified from the γ and q values are between states which happen to have the same nominal "l" values (as deduced from RMF [2] analysis of the series precursors) and, in the case of the interacting states of the two "nd" series, the same nominal "n" values as well. This is reminiscent of the *pure-precession* hypothesis, in which the interacting states differ by a single, pure atomic spin orbital, and in which the matrix elements of $A(r)$ and L_+ can be calculated explicitly. Although we know that the requirements of the pure-precession hypothesis cannot be satisfied completely for these Rydberg states because our analysis of the spin-orbit coupling in the $^2\Pi$ states demonstrates substantial l mixing, it is worthwhile now to explore how useful the pure-precession hypothesis might be in explaining the observed perturbations. Both the extent of its validity and the details of its breakdown promise to be informative.

The pure-precession model predicts the magnitudes of the Λ doubling and spin-rotation parameters as [32]

$$q=\frac{2B^2l(l+1)}{E_\Pi-E_\Sigma}\ , \tag{16}$$

$$p=\frac{2ABl(l+1)}{E_\Pi-E_\Sigma}\ , \tag{17}$$

and

$$\gamma=\frac{2ABl(l+1)}{E_\Pi-E_\Sigma} \tag{18}$$

where $E_\Lambda=T_0(\Lambda)$. Using these equations by substituting the energy denominators and integer, nominal l values for the dominant pairwise interactions identified above, we can calculate expected values for p, q, and γ. Table XI summarizes the observed and pure-precession predictions for the states in the $5.5<n^*<6.5$ group and for neighboring states.

Table XI indicates that the pure-precession model does

TABLE XI. Comparison between experimental spin-rotation and Λ-doubling constants and those calculated assuming pure precession for intermediate Rydberg states of CaF. Calculated values are obtained using pure precession equations [Eqs. (16)–(18)] with l equal to the nominal integer value, A_{SO} and B equal to their experimentally observed values, and ΔE determined from the ΔT_0 values for the dominant pairwise interactions discussed in the text. All values are in cm^{-1} units.

	γ		q		p[a]	
$n^{2S+1}\Lambda nl$	Expt.	Calc.	Expt.	Calc.	Expt.	Calc.
4.89 $^2\Sigma^+$ 6d	+0.0188(5)	+0.0115				
5.19 $^2\Sigma^+$ 6p	−0.0080(5)	−0.0156				
5.36 $^2\Pi$ 6d			+0.002 1(1)	+0.0022		+0.012
5.55 $^2\Sigma^+$ 8s	+0.002(2)	0				
5.88 $^2\Sigma^+$ 7d	+0.016(1)	+0.0114[b]				
5.98 $^2\Pi$ 8p			−0.000 72(7)	−0.0027		−0.015
6.19 $^2\Sigma^+$ 7p	−0.0078(6)	−0.0153				
6.35 $^2\Pi$ 7d			+0.004 8(1)	+0.0037		+0.012
6.55 $^2\Sigma^+$ 9s	+0.0035(3)	0				
6.88 $^2\Sigma^+$ 8d	+0.0130(6)	+0.0116[b]				
6.98 $^2\Pi$ 9p			−0.001 4(1)	−0.0042		−0.015
7.31 $^2\Pi$ 8d			+0.008 3(1)	+0.0057		+0.012
7.97 $^2\Pi$ 10p			−0.002 5(2)	−0.0062		−0.015
8.34 $^2\Pi$ 9d			+0.009 7(3)	+0.0087		+0.012

[a]The values of p are too small to be determined from our present data.

[b]The value of the spin-orbit constant for the $^2\Pi$ state assumed to be the unique perturber was not determined. An estimated value was obtained for use in Eq. (18) from Eq. (6) with $Z_o = 1.08$ and $Z_i(l) = 6.64$.

surprisingly well for most states at predicting q, p, and γ values from observed $T_0(\Lambda)$, A_{Π}, and B values. The observed γ values have the same signs as the calculated γ values for both the "nd" and the "np" $^2\Sigma^+$ series. They are 10–50 % larger than the calculated values for the "nd" series, but are only about half the magnitude of the calculated values for the states of the "np" series. While the observed γ values for states of the "ns" series are nonzero, they are only one-fourth of the magnitude of the smallest γ values from the other states, so they are closer to zero than those of either of the other two $^2\Sigma^+$ series. The calculated q values for $^2\Pi$ states increase approximately as n^{*3} due to the $1/n^{*3}$ dependence of the energy denominator and the n^* independence of B and l. The observed q values for the "nd" $^2\Pi$ states have the same sign as the calculated values and agree closely with them in magnitude. The observed q values of the "np" $^2\Pi$ states agree with the calculated q values in sign, but their magnitudes are about one-third of the calculated values.

Two assumptions of the pure-precession model are particularly worth examining for these states: (i) that each $^2\Pi$ state interacts with only one $^2\Sigma^+$ state and *vice versa* (the unique-perturber model) and (ii) that integer l values must be used in Eqs. (16)–(18). The pure-precession equations do a remarkably good job of predicting q and γ for the nominal "nd" states, but they do a poorer job for the "np" states. Thus at least one of the assumptions behind the model must be invalid. We could attempt to account for the observed parameter values by allowing noninteger, effective values of l to be used in place of the nominal, integer l values in Eqs. (16)–(18). The spin-orbit analysis has already made it clear that l mixing is quite strong in these states, making plausible such a replacement of integer l values by noninteger effective l values. However, relaxing the assumption of integer l values eliminates the only physical basis [$\Delta l = 0$ selection rules in the numerators of Eqs. (12)–(14)] for the simplification of the interactions among these three $^2\Sigma^+$ states and two $^2\Pi$ states of intermediate n^* into two unique-perturber pairings.

The major effect of l mixing is to allow additional interactions. We may guess at which secondary pairwise interactions are most important for the "l"$\neq 0$ states by examining the deviations of the experimental values of q and γ from the pure-precession model values. The most important secondary interactions are indicated by dashed arrows in Fig. 2. These are based on consistency of the sizes and signs of the energy denominators with the directions and magnitudes of the deviations of the parameter values from the pure-precession predictions.

However, any attempt to calculate p, q, and γ using Eqs. (16)–(18) under l-mixed conditions, allowing for multiple $^2\Sigma^+ \sim {}^2\Pi$ interactions and using effective l values derived from the $^2\Pi$ state spin-orbit analysis, is unlikely to succeed. Mixed-l states could be described as linear combinations of many atomic nl states,

$$|n^*\Lambda\rangle = \alpha|nl\rangle + \beta|n(l-1)\rangle + \cdots + \alpha'|n'l\rangle + \beta'|n'(l-1)\rangle + \cdots , \quad (19)$$

and the interaction matrix elements in Eqs. (12)–(14) will be sensitive to the signs and magnitudes of a potentially enormous number of unknown mixing coefficients. The spin-orbit analysis in Sec. IV B only determined the absolute magnitudes of generalized, interseries mixing coefficients for the $^2\Pi$ states. It revealed neither the signs

nor the intraseries n-mixing effects on the magnitudes of coefficients of the individual atomic orbitals. Moreover, the interseries l-mixing coefficients for the $^2\Sigma^+$ states are both unknown and unrelated to those for the $^2\Pi$ states. The exact deviations of fitted q and γ constants from pure-l predicted values cannot be accounted for by a *simple* generalization of a pairwise interaction model.

Another difficulty of extending the l-mixing results of the $^2\Pi$ series spin-orbit analysis to the $^2\Sigma^+ \sim {}^2\Pi$ rotational interactions is that the l-uncoupling interactions $(-BJ_+L_-)$ will be sensitive to the details of all lobes, not merely the innermost lobes, of the molecular orbitals. The evaluation of L^+ matrix elements, where all lobes of the wave function can contribute, will be much more complex than spin-orbit matrix elements, where only the inner lobes are heavily weighted. For the L^+ matrix elements, interference effects due to radial node mismatches between the wave functions of the interacting $^2\Sigma^+$ and $^2\Pi$ states are expected as a result of the different $nl \sim (n+1)l$ mixing patterns within each molecular series. These interferences profoundly affect the strength of the $^2\Sigma^+ \sim {}^2\Pi$ interaction, but the matrix elements are impossible to compute without accurate wave functions. In the absence of an *a priori* computation scheme for the γ and q parameters, an $s \sim p \sim d$ supercomplex deperturbation model will be required. This model would simultaneously account for the three observed γ values and the two pairs of observed $^2\Pi$ state (q, A) values by least-squares adjustment of four generalized l-mixing angles: one for the $p \sim d$ mixing between the two $^2\Pi$ series and three for the $s \sim p \sim d$ mixing among the three $^2\Sigma^+$ series [9].

The lowest-lying states of CaF, shown schematically in Fig. 3, present a pattern of nominally dominant interacting pairs of $^2\Sigma^+$ and $^2\Pi$ states which is quite different from that of the higher-energy Rydberg states. The six "valence" states, which correspond to the $5.5 \leq n^* \leq 6.5$ grouping of the Rydberg states discussed above by reason of having *approximately* the same quantum defects, are $X\,^2\Sigma^+$, $A\,^2\Pi$, $B\,^2\Sigma^+$, $B'\,^2\Delta$, $C\,^2\Pi$, and $F'\,^2\Sigma^+$. The primary $^2\Sigma^+ \sim {}^2\Pi$ interactions among this group of states are certainly not within nl complexes as defined by the nominal nl labels in Table I. Yet the unique-perturber condition of $p(^2\Pi) = \gamma(^2\Sigma^+)$ is clearly followed by the $A\,^2\Pi \sim B\,^2\Sigma^+$ pair and nearly as well by the $E\,^2\Sigma^+ \sim E'\,^2\Pi$ pair. Both of these pairs have been labeled "np" $^2\Pi \sim$ "$(n-1)d$" $^2\Sigma^+$ by RMF in their ligand-field analysis of the low-lying states. Strong $p \sim d$ mixing in both the "np" $^2\Pi$ and "$(n-1)d$" $^2\Sigma^+$ series makes these "Δl" $= \pm 1$ interactions possible. Moreover, the $A\,^2\Pi \sim B\,^2\Sigma^+$ and $E\,^2\Sigma^+ \sim E'\,^2\Pi$ unique-perturber pairs have energy denominators which are more than ten times smaller than those for any other possible $^2\Pi \sim {}^2\Sigma^+$ interactions. As a result of *energy-denominator selectivity,* the unique-perturber approximation becomes *accidentally* valid. The complexities due to multiple $^2\Pi \sim {}^2\Sigma^+$ interseries interactions, which are unavoidable in the $n^* > 5$ states, can be safely ignored for these low-lying states because of the heavy weighting of single, pairwise interactions by the energy denominators.

Figure 4 illustrates a major departure of the γ constants for the $B\,^2\Sigma^+$ and $E\,^2\Sigma^+$ states from the simple scaling (independent of n^*) relationship. There is a corresponding glitch in the q constants for the $A\,^2\Pi$ and $E'\,^2\Pi$ states. The explanation for these deviations is illustrated by Fig. 3; it is an energy denominator rather than a $^2\Pi$-$^2\Sigma^+$ interaction-matrix-element effect. At $n^* \approx 1.9$ the unique perturber of the "$4d$" $^2\Pi$ state is the "$3d$" $^2\Sigma^+$ where the $^2\Sigma^+$ state lies above the $^2\Pi$ state. At $n^* \approx 2.9$ the "$5p$" $^2\Pi$ state is uniquely perturbed *from below* by the "$4d$" $^2\Sigma^+$ state. Finally, at $n^* \approx 6.1$ the "$8p$" $^2\Pi$ state is dominantly perturbed *from above* by the "$7p$" $^2\Sigma^+$ state. The changes in sign of the energy denominator and in the identity of the dominant perturber are a simple consequence of the relatively large changes in quantum defects that occur for the lowest members of each Rydberg series. By $n^* \approx 5$, the core-penetrating Rydberg series have settled into their asymptotic ordering within s-p-d supercomplexes and, above $n^* \approx 5$, it is expected that the fine-structure parameters will follow approximate scaling laws.

The fundamental conclusions of the present analysis of Λ-doubling and spin-rotation interactions for the intermediate-n^* Rydberg states are that l mixing is very much in evidence and that exclusive pairwise $^2\Pi$-$^2\Sigma^+$ interactions are not sufficient to explain quantitatively the

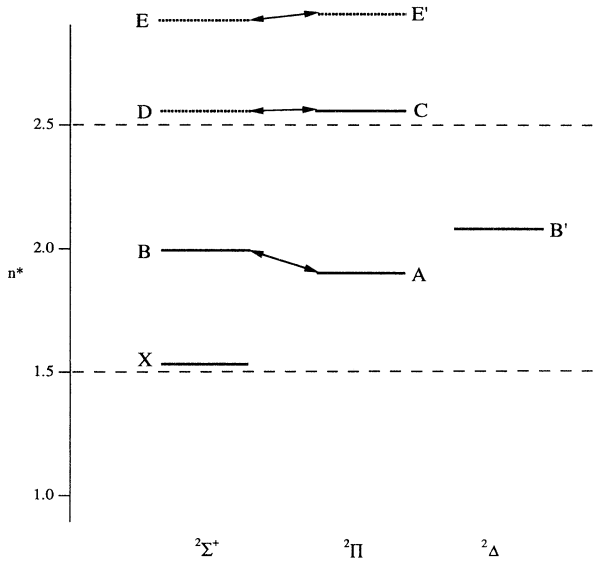

FIG. 3. Energies of the lowest states of CaF plotted vs n^*. Dashed horizontal lines indicate the range of quantum defects of the group of states highlighted in Fig. 2. Levels drawn as solid lines are low-energy states which correspond to that grouping. Levels shown as dashed lines are those which correspond to states which are outside of the $5.5 < n^* < 6.5$ grouping. Pairwise interactions deduced from the Λ-doubling and spin-rotation constants are indicated by arrows. This figure also demonstrates the energy shifts which occur at low n^*. The $A\,^2\Pi$ state is below the $B\,^2\Sigma^+$ state; however, in the next higher-n^* group the $^2\Pi$ state (the E' state) is above the $^2\Sigma^+$ state (the E state). This energy ordering persists for all groups of states at higher n^*. This low-n^* energy reordering explains the large low-n^* deviation of γ shown in Fig. 4.

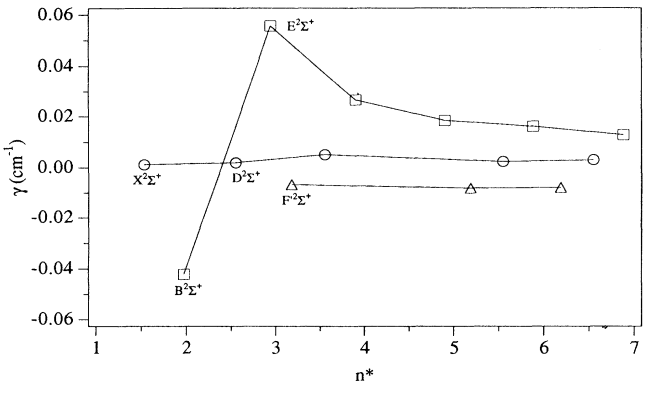

FIG. 4. Spin-rotation constant vs n^*. This figure shows how γ displays the expected scaling relationship. The energy reordering, which is the reason for the large deviation at low n^*, is illustrated in Fig. 3.

values of the observed parameters. The deviations of the γ and q constants from calculated pure-precession values can be rationalized by postulating one secondary "$\Delta l \neq 0$" interaction. However, the proper way to treat this problem quantitatively will be through simultaneous analyses of the entire interacting $s \sim p \sim d$ supercomplex of states using a multistate effective-Hamiltonian matrix model [7]. These supercomplex deperturbation analyses are currently being carried out [9].

We have ignored the Λ doubling of the $^2\Delta$ states because this effect clearly cannot be explained by a two-state interaction. The interactions responsible for Λ doubling in $^2\Delta$ states occur at fourth order of perturbation theory. Nevertheless, the members of the $\mu = 0.86$ $^2\Delta$ series do show measurable Λ doubling in our spectra, particularly as n^* increases. The sign of the $q(J+\frac{1}{2})^4$ term is negative and the p constant is undetermined for the two $^2\Delta$ states for which we have been able to extract values of Λ-doubling parameters from the data (Table IV). The magnitude of q increases with n^*, as expected. If the magnitude of q were due to a fourth-order effect, the $q(J+\frac{1}{2})^4$ Λ-doubling term would be expected to scale as n^{*9}. More physically, the appearance of Λ doubling in $^2\Delta$ states signals the breakdown of a Hund's case (a) or (b) perturbation expansion. The l-uncoupling effects in the higher-n^* $s \sim p \sim d$ supercomplexes cause rapid evolution (as J increases) toward Hund's case (d), where the usual p, q, and γ fine-structure parameters become meaningless. It is inevitable that any fine-structure parameter expected to scale as n^{*x} will, if $x > 1$, be replaced at high-n^* by a direct first-order interchannel-interaction parameter. The Λ-doubling effects in the $^2\Delta$ states are being treated by an $s \sim p \sim d$ supercomplex deperturbation model [9].

V. CONCLUSIONS

The effective-Hamiltonian parameters for the newly observed intermediate-n^* $^2\Sigma^+$, $^2\Pi$, and $^2\Delta$ Rydberg states of the CaF molecule have been determined and interpreted. The molecular constants reported here confirm the nominal n, l, and λ series assignments and the value of the ionization potential we reported previously [1]. But more importantly, we have used the fine-structure parameters to develop a comprehensive picture of the core-penetrating series of the CaF molecule. n^*-based scaling relationships for the molecular constants are crucial to this picture. Scaling relationships provide compact descriptions of most of the properties of the large number of observed Rydberg states. The effective Hamiltonian parameters, which vary sensibly along each series, were used to show quantitatively how the core-penetrating Rydberg series connect to the ligand-field model developed for the valence states [2]. Spin-orbit, Λ-doubling, and spin-rotation parameters were most useful in describing how the various Rydberg-series orbitals collapse onto the $(CaF)^+$ molecular ion core in their respective valence terminus state.

The scaling relationship for the molecular spin-orbit parameters was developed by adapting the exact hydrogenic expression, Eq. (2), for the (n,l) dependence of the spin-orbit splitting. Our generalization of the hydrogenic (n,l) scaling law incorporates empirical adjustments which are patterned after those which have been employed for nonhydrogenic atomic ions [28,29]. The effective charge $Z_i(l)$ accounts for the charge experienced within the Ca^{2+} atomic ion core by the innermost lobe of the Rydberg orbital, where the spin-orbit interaction takes place. The effective charge Z_o accounts for the average $(CaF)^+$ molecular ion core charge, which controls the size of the outermost lobes.

We have interpreted the charge experienced by the innermost lobes of a π Rydberg orbital by direct comparison with the analogous charge experienced by the p and d Rydberg orbitals of the Ca^+ atomic ion. The effective shielding of the outer lobes of the molecular Rydberg orbital from the Ca^{2+} atomic ion core by F^- was determined by adjusting the effective $(CaF)^+$ core charge so that the effective charges seen by the innermost lobes of the CaF π Rydberg orbitals could be interpreted solely in terms of the mixing of Ca^+ p and d Rydberg orbitals [$nl \sim n(l+1)$ mixing]. The resulting π $p \sim d$ mixing coefficients are quite close to those determined by RMF for the valence states using a ligand-field model [2]. The derived value of the molecular ion core effective charge $Z_o = 1.08$ illustrated the incomplete shielding of the inner several lobes of the Rydberg orbital from the Ca^{2+} core by F^-. In the context of expansion of the molecular Rydberg orbitals in terms of Ca^+ atomic orbitals, Z_o differs from $+2$ due to the substantial effects of $nl \sim (n+1)l$ mixing induced by the shielding effects of F^-. Using the Z_o value from the analysis of the $^2\Pi$ states, we have shown that the $^2\Delta$ states are derived almost entirely from Ca^+ nd orbitals. The spin-orbit scaling coefficients show no evidence of l mixing in the innermost lobes for the $^2\Delta$ states. However, the fact that $Z_o = 1.08$ rather than 2 again points to significant $nl \sim (n+1)l$ mixing of the Ca^+ basis states in the $^2\Delta$ Rydberg states as well.

The two $^2\Pi$ and one $^2\Delta$ valence (series terminus) states have spin-orbit constants which are much larger than scaling predictions. We have interpreted this as being

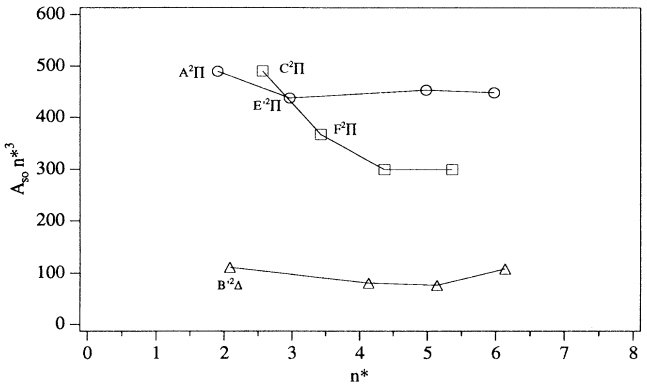

FIG. 5. $A_{SO} \times n^{*3} n^{*}$. This figure demonstrates the n^* scaling of the spin-orbit constant. The spin-orbit constant follows the expected n^{*3} dependence at $n^* > 4$. The deviations at low n^* are explained as due to reverse polarization effects.

due to a decrease in effective F^- shielding (increase in Z_o) as the Rydberg orbital becomes smaller, or in the context of the Ca^+ basis-state expansion, as being due to a change in the $nl \sim (n+1)l$ mixing at low n^* because no Ca^+ states of a smaller nominal n are available for interactions. The additional effects of orbital overlap with the filled F^- $2p$ orbitals are estimated, and a 4% contribution from the F^- $2p$ orbital was shown to account for the unique increase of the spin-orbit scaling coefficient for the $C\,^2\Pi$ state. Although we have shown that this effect of overlap with F^- $2p$ should persist throughout this Rydberg series, the fitted constants show that this contribution does not scale smoothly with n^*.

Scaling relationships for the measured γ and q parameters, which arise from $^2\Pi \sim {}^2\Sigma^+$ interactions, were also developed. These parameters were shown to be consistent with significant $l \sim l+1$ and $n \sim n+1$ mixing in the primitive Ca^+ basis, thus demonstrating the importance of multiple interseries interactions. An $s \sim p \sim d$ supercomplex deperturbation, using a multistate effective Hamiltonian matrix, will be required to characterize the important l-mixing interactions. That analysis is in progress [9] and will be reported separately.

The scaling relationships discussed here describe the intermediate-n^* core-penetrating Rydberg states of the CaF molecule. However, the molecular constants for the lowest states of each series deviate from values predicted by scaling relations (see Figs. 4 and 5). The deviations from scaling predictions provide important clues about what happens when the Rydberg orbital starts to collapse into the core [6]. For example, the rotation and vibration constants decrease appreciably as n^* decreases, and this provides information about the contribution of the single electron outside of closed shells to the bonding in the CaF molecule. As the Rydberg orbital collapses into the core, it partially shields the Ca^{2+} ion from the F^- ion and thereby weakens the bond. This effect, in particular the absence of any low-n^* states with ω and B values larger than those of the CaF^+ $X\,^1\Sigma^+$ state, suggests that the bonding in CaF is purely ionic. Covalent contributions to bonding would cause the rotation and vibration constants to increase for some of the low-n^* states.

The low-n^* deviations of the molecular constants from scaling predictions also provide information about the Ca^{2+}-centered orbital polarization of the different core-penetrating Rydberg series. At the crossover from the Rydberg picture, where the electron "sees" a $+1$ point-charge potential, to the valence picture, where the electron is in a Ca^{2+}-centered orbital perturbed by a point charge (the RMF picture), the quantum defects of the low-energy states shift relative to those of the higher series members by amounts which depend on the sign and magnitude of the orbital polarization in a given series [6]. This results in accidental degeneracies between some of these low-n^* states. These atypical energy differences lead to large deviations and even a sign reversal of the spin-rotation constants in the "nd" $^2\Sigma^+$ series. These breakdowns of scaling are due to energy-denominator effects, not to matrix element effects.

ACKNOWLEDGMENTS

The authors would like to thank A. J. Merer, Ch. Jungen, Z. Jakubek, L. Kaledin, and C. Gittins for useful discussions. We also thank W. E. Ernst and R. F. Barrow for communicating their results to us prior to publication. This work was supported by the National Science Foundation under Grants Nos. PHY87-09759 and CHE91-20339.

*Present address: Los Alamos National Laboratory, Los Alamos, NM 87545.

†Present address: Battelle, Pacific Northwest Laboratories, P.O. Box 999, Richland, WA 99325.

‡Author to whom correspondence should be addressed.

[1] J. E. Murphy, J. M. Berg, A. J. Merer, N. A. Harris, and R. W. Field, Phys. Rev. Lett. **65**, 1861 (1990).

[2] S. F. Rice, H. Martin, and R. W. Field, J. Chem. Phys. **82**, 5023 (1985).

[3] T. Törring, W. E. Ernst, and J. Kändler, J. Chem. Phys. **90**, 4927 (1989).

[4] J. d'Incan, C. Effantin, A. Bernard, J. Verges, and R. F. Barrow, J. Phys. B **24**, L71 (1991).

[5] C. M. Gittins, N. A. Harris, R. W. Field, J. Verges, C. Effantin, A. Bernard, J. d'Incan, W. Ernst, P. Bündgen, and B. Engels, J. Mol. Spectrosc. (to be published).

[6] N. A. Harris and R. W. Field, J. Chem. Phys. **98**, 2642 (1993).

[7] G. Herzberg and Ch. Jungen, J. Mol. Spectrosc. **153**, 81 (1972).

[8] R. S. Mulliken, J. Am. Chem. Soc. **86**, 3183 (1964).

[9] J. E. Murphy, Ph.D. thesis, Massachusetts Institute of Technology, 1992.

[10] P. F. Bernath and R. W. Field, J. Mol. Spectrosc. **82**, 339 (1980).

[11] C. E. Hamilton, J. L. Kinsey, and R. W. Field, Annu. Rev. Phys. Chem. **37**, 493 (1986).

[12] D. Hildenbrand and E. Murad, J. Chem. Phys. **44**, 1524

(1966).
[13] L. T. Earls, Phys. Rev. **48**, 423 (1935).
[14] J. Nakagawa, P. J. Domaille, T. C. Steimle, and D. O. Harris, J. Mol. Spectrosc. **70**, 374 (1978).
[15] A. A. Kitaev, I. S. Gotkis, P. G. Val'kov, and K. S. Krasnov, Khim. Fiz. **7**, 1685 (1988).
[16] D. Hildenbrand (private communication).
[17] J. A. Coxon, J. Mol. Spectrosc. **58**, 1 (1975).
[18] A. J. Kotlar, R. W. Field, J. I. Steinfeld, and J. A. Coxon, J. Mol. Spectrosc. **80**, 86 (1980).
[19] J. M. Brown, A. S.-C. Cheung, and A. J. Merer, J. Mol. Spectrosc. **124**, 464 (1987).
[20] P. Büdgen, B. Engels, and S. D. Peyerimhoff, Chem. Phys. Lett. **176**, 407 (1991).
[21] W. E. Ernst and J. Kändler, Phys. Rev. A **39**, 1575 (1989).
[22] W. J. Childs, G. L. Goodman, and L. S. Goodman, J. Mol. Spectrosc. **86**, 365 (1981); G. Weiler, Diplom thesis, Freie Universität Berlin, 1986.
[23] M. Dulick, P. F. Bernath, and R. W. Field, Can. J. Phys. **58**, 703 (1980).
[24] J. Verges, C. Effantin, A. Bernard, A. Topouzkhanian, A. R. Allousche, J. d'Incan, and R. F. Barrow, J. Phys. B **26**, 279 (1993).
[25] W. E. Ernst, J. Kändler, and O. Knüppel, J. Mol. Spectrosc. **153**, 81 (1992).
[26] P. F. Bernath and R. W. Field, J. Mol. Spectrosc. **82**, 339 (1980).
[27] C. A. Fowler, Phys. Rev. **59**, 645 (1941).
[28] B. Edlén, in Encylopedia of Physics Vol. 27 (Springer-Verlag, Berlin, 1964), p. 107.
[29] A. Landé, Z. Phys. **25**, 46 (1924).
[30] J. Sugar and C. Corliss, J. Phys. Chem. Ref. Data Suppl. 2 **14**, 74 (1985).
[31] R. Pitzer (private communication).
[32] H. Lefebvre-Brion and R. W. Field, *Perturbations in the Spectra of Diatomic Molecules* (Academic, Orlando, 1986).